A R C H I V E S O F M E T A L L U R G Y A N D M A T E R I A L S
Volume 51 2006 Issue 1

H. PAUL*, **, J. H. DRIVER***, C. MAURICE***, M. BIJAK*

LARGE STRAIN DEFORMATION SUBSTRUCTURES AND LOCAL CRYSTALLOGRAPHY IN {100}<001>/{110}<001> ALUMINIUM BICRYSTALS

MIKROSTRUKTURA I MIKROTEKSTURA ODKSZTAŁCONYCH BIKRYSZTAŁÓW ALUMINIUM O UKŁADZIE ORIENTACJI KRYSZTAŁÓW {100}<001>/{110}<001>

Symmetrically oriented bicrystals of pure Al(99.998%) have been deformed in channel-die compression up to strains of ~1.5 to correlate the dislocation substructures and the slip system distributions. The study has focused on structure development in {100}<001>/{110}<001> (cube/Goss) – oriented bicrystals with the grain boundary situated parallel to the compression plane. Both orientations have the same nominal Taylor factor and deform macroscopically by the same amount but have stable (Goss) and unstable (cube) micro-deformation behavior. The character of the deformation substructure was determined by systematic local orientation measurements using high resolution EBSD in a SEM-FEG scanning electron microscope and also by transmission electron microscopy (TEM) and the CBED technique at specific locations. The bicrystal deformation analysis shows that the microtexture evolution within neighboring grains is quite different. Very strong deformation banding is observed within crystallites with the unstable orientation, i.e. cube-oriented grain forms classical deformation bands of slightly and strongly dislocated areas. The Goss-oriented grains within bicrystals are more stable under plane strain conditions and do not show any tendency to strain inhomogeneties except for the zone near the grain boundary.

Keywords: Aluminium bicrystals; Texture; Deformation; Orientation microscopy;

W pracy analizowano umocnieniowe zachowanie się bikryształów Al(99.998%) o orientacji krystalitów {100}<001>/{110}<001>, odkształcanych w próbie nieswobodnego ściskania do zakresu odkształceń ~1.5. Granica rozdziału pomiędzy ziarnami usytuowana była równolegle do płaszczyzny ściskania. Obydwa krystality formujące bikryształ scharakteryzowane są tę samą wartością współczynnika Taylora. Jednakże ich zachowanie umocnieniowe jest odmienne, tj. orientacja {110}<001> pozostaje stabilna podczas gdy {100}<001> jest silnie niestabilna. W oparciu o pomiary orientacji lokalnych w TEM a także z wykorzystaniem techniki EBSD w SEM wyposażonym w działo o emisji polowej dokonano charakterystyki mikrostrukturalnej i tekturowej. W krystalicie o orientacji {100}<001> obserwowano formowanie się pasm odkształcenia złożonych z obszarów o wysokiej i niskiej gęstości dyslokacji. Orientacja G{110}<001> pozostawała stabilna nie przejawiając tendencji do formowania pasmowych niejednorodności odkształcenia za wyjątkiem wąskich obszarów w pobliżu granicy pomiędzy ziarnami.

1. Introduction

The microstructural and microtextural response of plastically deformed fcc metals and alloys has been extensively studied over the last few decades. Previous investigations have been performed on single crystals e.g. [1-4], some have been carried out on bicrystals e.g. [5-9] and polycrystals [10-12], including also extremely coarse grained polycrystalline aggregates [13]. Of particular interest in rolled polycrystalline materials are the crystal orientations which appear in a material obtained in horizontal continuous casting process. The as-cast (extremely coarse grained) structure reveals usually pronounced {100}< *uvw* >-fibre texture and is significantly different when compared with conventional hot rolled band. This is clearly visible in copper and copper-base alloys [14].

The effect of the mutual interaction between different orientations on the deformation response and recrystallization behavior can most basically be explored by examining bicrystals. Specimens composed of bicrystals with well-defined orientations obviously enable one to examine the characteristic deformation of individual

* INSTITUTE OF METALLURGY AND MATERIALS SCIENCE, 25 REYMONTA ST, 30-059 KRAKÓW, POLAND
** UNIVERSITY OF ZIELONA GÓRA, MECHANICAL DEPARTMENT, 65-246 ZIELONA GORA, 50 PODGÓRNA ST., POLAND
*** ECOLE NATIONALE SUPERIEURE DES MINES DE SAINT ETIENNE, CENTRE SMS, 158 COURS FAURIEL, 42023 SAINT ETIENNE CEDEX 2, FRANCE

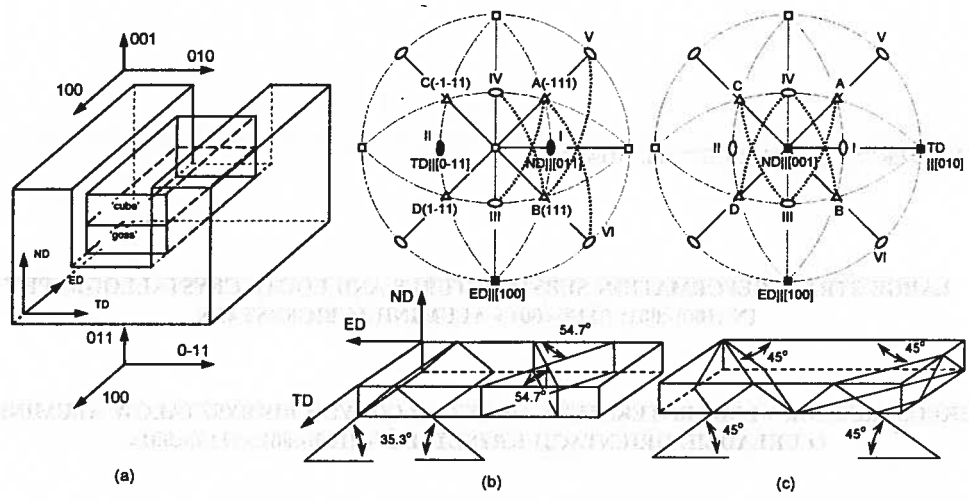

Fig. 1. (a) The crystallographic directions within 'cube' and 'Goss'– oriented grains and the situation of the grain boundary, (b) and (c) stereographic (001) projection showing the active slip systems in channel-die compressed bicrystal: (b) Goss(011)[100] and (c) cube(001)[100] – oriented grains, respectively

grains and the role of the strain heterogeneities near the grain boundary with their influence on nucleation of recrystallization. Aluminium has been used in most of these cases [6, 8, 9, 15, 16], but some of the investigations have been carried out e.g. on other pure metals: copper [17], silver [18], magnesium [19], or alloys: β-brass [20], Fe-3%Si [21].

The purpose of this paper is to examine the influence of grain orientations and active slip systems on the deformation microstructure and microtexture evolution during plane strain compression in aluminium bicrystals with high symmetry orientations. The grain orientations {110}<001>/{100}<001> (Goss/cube), representing stable vs. unstable deformation behavior with the same nominal value of Taylor factor of $\sqrt{6}$, have been deformed in channel-die compression to a strain of about 1.5. The deformation behaviour of individual Al crystals during plane strain compression has shown that the Goss{110}<001> orientation is stable up to very large strains [1]. The unstable cube{100}<001> orientation very quickly breaks up into differently oriented areas [16, 22, 23].

The geometry of deformation for these bicrystals was such that the bicrystals boundary, which separates the top and the bottom crystals at the midthickness of the specimen, lies parallel to the compression plane, i.e. {100} and {110} for cube and Goss-oriented grains, respectively. The <100> direction, within both crystallites, is aligned with the channel. The die constraints deformation are aligned in the <100> and <110> directions, for the cube and the Goss-oriented grains, respectively (Fig. 1).

The deformation microstructures and microtextures were characterized over a wide range of scales using a combination of optical metalography and scanning (SEM) and transmission (TEM) electron microscopes. The use of aluminium, with a high stacking fault energy (SFE) excludes mechanical twinning and facilitates identifying the mechanisms responsible for texture evolution during plane strain deformation.

2. Experimental Procedures

2.1. Material and methods

Aluminium bicrystals with the following grain orientations of {110}<001>/{100}<001> (Goss/cube) were selected. The bicrystals with controlled orientations were grown by the modified Bridgman technique (horizontal solidification), using split graphite moulds, at the Ecole des Mines de Saint Etienne, from high purity metal (99.998%). The dimensions of the bicrystals were approximately 15 mm (thickness) × 22 mm (width) × 150 mm (length). The orientations of the crystallites before compression were checked by back reflexion Laue X-ray. The samples were compressed in a channel-die rig at 77 K and at a nominal strain rate of $\sim 10^{-4} s^{-1}$. Teflon films were used as a lubricant and periodically replaced at deformation intervals of about 0.2.

Optical microscopy of the internal microstructure was carried out using polarized light on anodized sections (in 2% HBF_4 acid solution). The deformed speci-

mens were mostly examined in a scanning electron microscope JEOL JSM 6500F equipped with a field emission gun – SEMFEG). Microscope control, pattern acquisition and solution were carried out with the HKL Channel 5 system. The diffraction data were acquired as orientation maps using raster scans of 400×300 pixels, with different step sizes within the range of 0.1-0.5 μm. The deformed samples were prior mechanically polished to remove any surface-induced deformed effects and then electropolished in a solution containing 20% nitric acid in methanol, at –35°C and a voltage within the range of 12-14 V. The samples were also examined by TEM using a 200 kV Philips CM 200 and semi-automatic Kikuchi pattern analysis. The samples were sectioned in the ED-ND plane (where: ED – extension direction, ND – normal direction) by wire cutting for thin foil preparation. The thin TEM foils have been prepared by a twin-jet technique in a solution composed of 20% nitric acid, 75% methanol with addition 5% of glycol, at –35°C and a voltage of 20.5 V, using TenuPol-5. Each TEM sample had a very large thin area. The majority of metallographic observations and local orientation measurements were made on the longitudinal plane, i.e. ND-ED, with additional inspection of the ND-TD sections (where: TD – transverse direction).

The situation of the bicrystals in the channel-die device and the nominal orientations of the grains are shown in Fig. 1a. The configuration is such that the bicrystal boundary plane is nearly perfectly parallel to the compression plane. Figures 1b and c show stereographic projections on (001) plane. The positions of the external axes and the most active slip systems (Schmid-Boas notation is applied) in channel-die compressed single crystals (for Goss- and cube orientations) are marked. The interrelation between the grain orientations forming a bicrystal, could be described as:

$$\{100\}\langle 001\rangle/\{110\}\langle 001\rangle(\{100\}\langle 001\rangle)$$

$$45°\langle 100\rangle \parallel ED \leftrightarrow \{110\}\langle 001\rangle$$

2.2. Initial geometry of slip

The rotation tendencies of particular crystallites forming bicrystals are mainly determined by the situation of the active slip systems. Theoretical predictions of the deformation behavior and the evolution of the initial grains orientation are strongly dependent on the adopted state of stress or deformation. In Tucker's approach [24] the state of stress for the channel-die compression is described as a superposition of uniaxial tension and compression, for which it is assumed: $\sigma_{ED/ED} = -\sigma_{ND/ND}$, and $\sigma_{TD/TD} = \sigma_{TD/ED} = \sigma_{ND/TD} = \sigma_{ND/ED} = 0$. In accordance with this assumption, the value of Schmid's factor on all possible slip systems for two considered orientations (Table I) was calculated from the dependence:

$$w_s = \tau/\sigma = \cos\alpha_c \cos\beta_c - \cos\alpha_e \cos\beta_e,$$

where: α_c, β_c – angles between the vector normal to the slip plane and the axes of compression and tension, and α_e, β_e – angles between the vector of the slip direction and the axes of compression and tension.

TABLE

The value of the Schmid's factor for selected orientations on all slip systems of {111}<011>-type. Tucker's [24] state stress is assumed

Crystal orientation	Slip systems											
	(111)		[$\bar{1}\bar{1}$1]			[$\bar{1}$11]			[1$\bar{1}$1]			
	[01$\bar{1}$]	[$\bar{1}$01]	[1$\bar{1}$0]	[0$\bar{1}\bar{1}$]	[101]	[$\bar{1}$10]	[01$\bar{1}$]	[101]	[$\bar{1}\bar{1}$0]	[0$\bar{1}\bar{1}$]	[$\bar{1}$01]	[110]
Slip system (B-H)	*a1*	*a2*	*a3*	*b1*	*b2*	*b3*	*c1*	*c2*	*c3*	*d1*	*d2*	*d3*
Slip system (S-B)	*B2*	*B4*	*B5*	*C1*	*C3*	*C5*	*A2*	*A3*	*A6*	*D1*	*D4*	*D6*
Goss (110)[001]	0.00	0.82	0.82	0.00	0.41	0.41	0.00	0.82	0.82	0.00	0.41	0.41
Cube (100)[001]	0.41	0.82	0.41	0.41	0.82	0.41	0.41	0.82	0.41	0.41	0.82	0.41

where: B-H – Bishop-Hill and S-B – Schmid-Boas notations.

The results of these calculations, showing highly stressed slip systems, are presented schematically on stereographic projections (in crystal coordinates) in which the dominating slip systems for each orientation are marked (Fig. 1b and c).

Single crystals calculations show that the Goss(011)[100] orientation remains stable in a wide range of deformations. At the initial deformation stages the most active slip systems, forming co-planar pairs, are operating on planes A($\bar{1}$11) and B(111), situated symmetrically with respect to plane perpendicular to ED (Fig.1b). The normals of the most active slip planes form an angle of 35.3° with respect to ND. The next two planes of C($\bar{1}\bar{1}$1) and D(1$\bar{1}$1), are less privileged for dislocation motions in the deformation process and they are situated perpendicular to the compression plane.

The stability of this orientation remains in accordance with the theoretical predictions, both by full constraints (FC) Taylor's model – not allowing the occurrence of shears in the direction of elongation, and by partly relaxed constraints (RC) Taylor's model – accepting the occurrence of shears in the direction of elongation. The cube(100)[001] orientation is strongly unstable. In these grains on each {111} slip plane, one slip system with the highest values of the Schmid factor of 0.82 is potentially active (Table 1). At the beginning of deformation all {111} planes are inclined at 45° with respect to all external axes. Starting from the early deformation stages this orientation undergoes decomposition connected with the formation of band-like inhomogeneities (deformation bands). This is responsible for the limited rotation of a separated volume of the matrix [9, 22]. In particular, the superposition of two selected rotations of the crystal lattice about <112>-type axes can lead, in a channel-die compression mode ($\varepsilon_{TD/TD} = 0$), to the summary rotation about the <100> direction parallel to TD.

3. Experimental results

3.1. Macroscopic observations and global texture evolution

Visual inspection of anodized surfaces reveals microstructural details in the longitudinal plane at finish logarithmic strain level of 1.5. It is visible that both crystals accommodate nearly the same amount of strain up to the relatively high deformation degrees, probably as a result of the same value of the Taylor factor.

The most characteristic feature of the deformation microstructure of a cube {100}<001> crystal is the formation of the band-like heterogeneities of deformation (Fig. 2a-c). The process of bands formation increases greatly with the strain so that after 1.5 (68%) deformation they penetrate the whole volume of the crystallite, but still do not show any tendency to intersect the grain boundary. The distribution of slips in a Goss {110}<001>-oriented crystallite is significantly more homogeneous (Fig. 2a, c and d). For the deformation applied here, this crystallite does not show any significant tendency to produce strain heterogeneities, excluding the thin layer at the grain boundary, where accommodation bands are observed (Fig. 2a and c).

The final microtextures of the particular crystallites forming bicrystals, obtained by SEMFEG/EBSD line scans (for very large – few mm line scan) and presented as a {111} pole figures, shown relatively high stability of the Goss-oriented grains (Fig. 3a). In the case of unstable, cube orientation, different tendencies of scattering occur probably as a result of the different slip systems operation, on different slip planes (Fig. 3b). Hence, the {111} pole figure exhibits relatively wide orientation spread, typical of the analyzed unstable orientation.

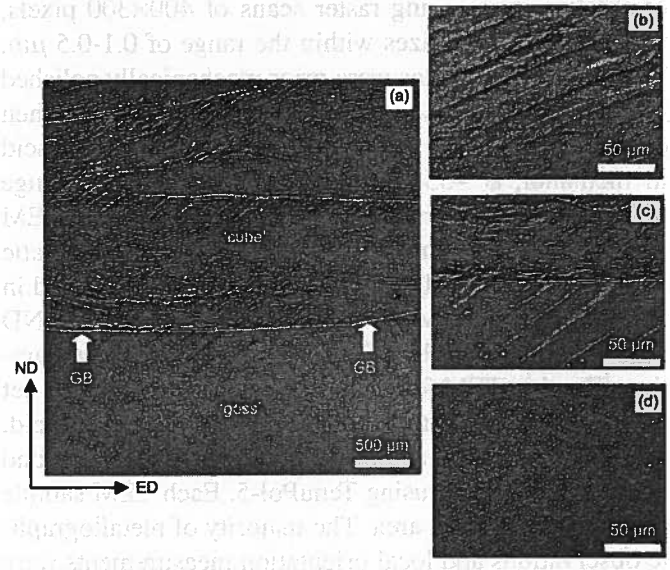

Fig. 2. (a) Global view on microstructure near the grain boundary at strain level of 1.5, and details from particular places: (b) cube-oriented grain, (c) area near grain boundary, (d) Goss-oriented grain. Optical microscopy on ND-ED plane

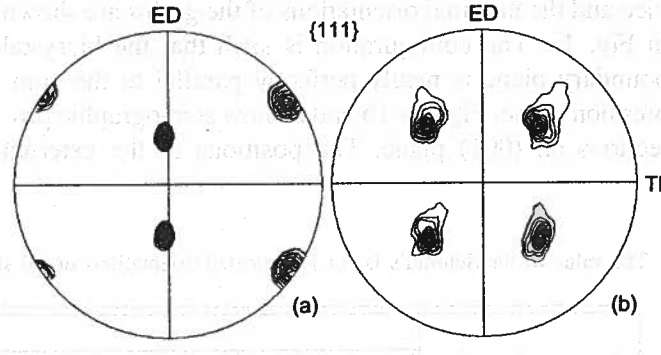

Fig. 3. Texture formation in particular grains forming bicrystals in samples deformed to strain of 1.5: (a) Goss- and (b) cube-oriented grains, respectively. Large area orientation scans by SEMFEG/EBSD. Step scan of 0.5 μm

3.2. TEM microstructure and microtexture

The TEM microstructure and microtexture analysis on samples taken from the longitudinal plane can provide the information about some detailed features of individual cell orientations with dimensions down to tens of nanometers and it clearly shows that both crystals form quite different dislocation substructures.

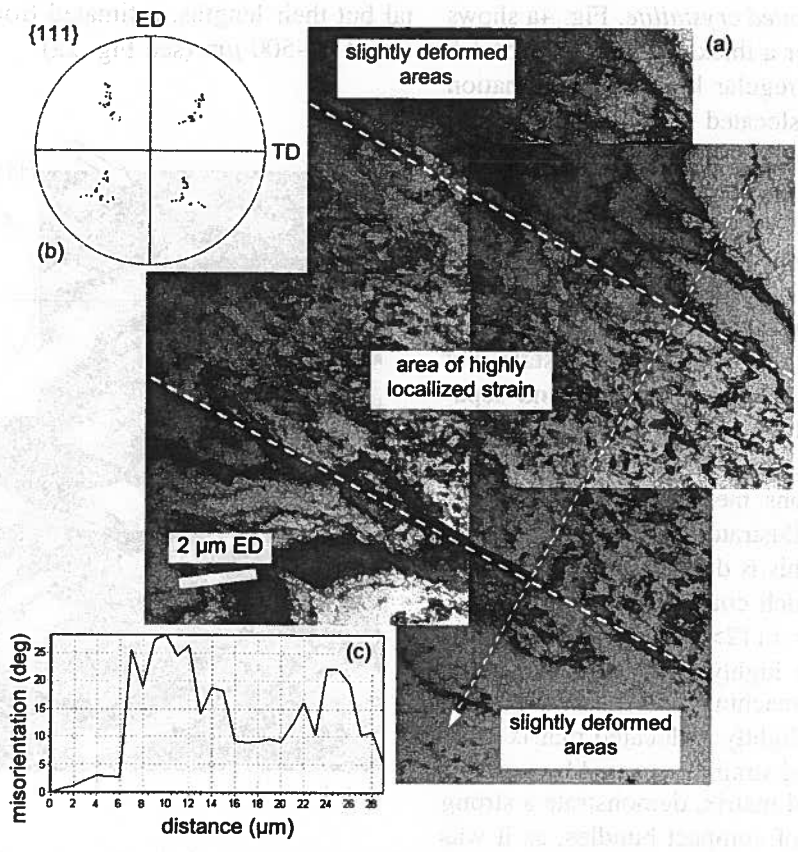

Fig. 4. Deformation bands in cube grain. (a) TEM microstructure at the nominal deformation of 1.5, and (b) corresponding {111} pole figure and (c) misorientation profile across the band. TEM local orientation measurements

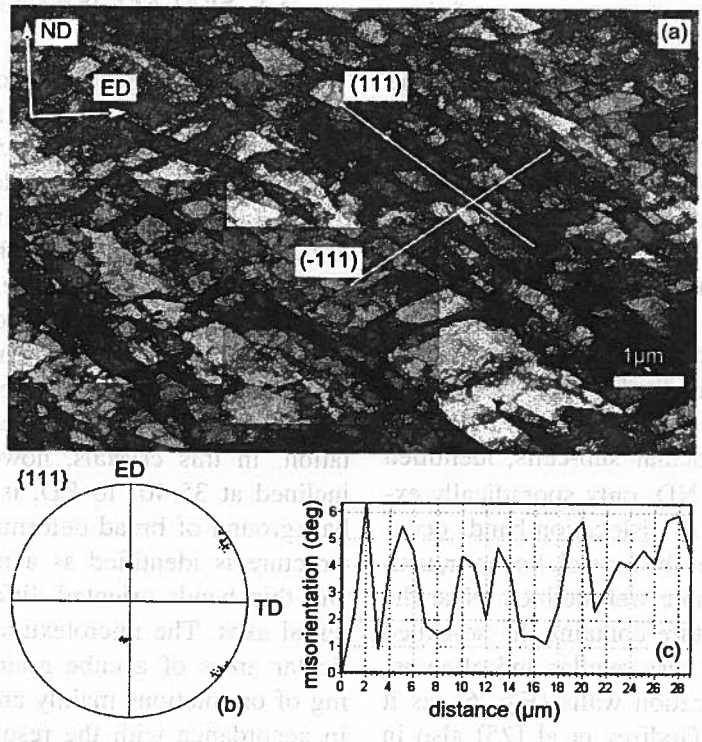

Fig. 5. Elongated cell substructure in Goss-oriented crystallite. (a) TEM microstructure at the nominal deformation of 1.5, and (b) corresponding {111} pole figure and (c) misorientation profile along ND. TEM local orientation measurements

Cube{100}<001>-oriented crystallite. Fig. 4a shows a TEM microstructure after a thickness reduction of 1.5 (68%); it is composed of regular layers of deformation bands separated by less dislocated matrix. It is apparent that the typical deformation bands observed here have a width in the range of 1-5 μm, and they are composed of only slightly elongated and strongly 'diffused' sub-cells. The later is due to low temperature deformation (77 K). In agreement with the optical micrographs, the bands have different angles with respect to ED; typically 0-35°. They do not run completely through the crystals, but terminate in relatively broad zones (blocks) and separate the areas in which different slip systems operate. The {111} pole figure (Fig. 4b), constructed on the basis of the local orientations measured along two line scans across the bands, illustrates the tendency of the microtexture scattering. This is described as a summary TD(|| <100>) rotation which could result from the superposition of two or four <112>-type rotations around axes lying near TD. The highly dislocated bands are associated with rotation reaching 25-30° with respect to the neighboring, only slightly dislocated matrix (Fig. 4c). The bands of localized strain, separated by areas of relatively weakly deformed matrix, demonstrate a strong tendency to form groups of compact bundles, as it was previously observed by Paul & Driver [9] in cube grains from {100}<001>/{110}<011>-oriented bicrystals.

Goss{110}<001>-oriented crystallite. A typical, well-defined cellular dislocation structure, generated within this orientation, is shown in Fig. 5a. This microstructure consists of two complementary sets of elongated bands, inclined at ±35° to ED. Both sets of dislocation walls marking the bands lie very close to the expected traces of the active {111} slip planes for this orientation. They are inclined anti- (–35°) and clockwise (+35°) to ED. As a result of their intersection the rectangular cells, with dimensions of 0.2-0.8 μm, are formed. The dislocation cell walls occur along the trace of the two (111) and ($\bar{1}$11) planes, in which slip systems of (a2, a3) and (c2, c3) operate, for the positive and negative inclined dislocation walls, respectively. This microstructure is characterized by a relatively small orientation spread, clearly visible in Fig. 5b. The misorientation angle formed between the particular sub-cells, identified along a line scan parallel to ND, only sporadically exceeds 10° (Fig. 5c). Each set of dislocation bands occupies nearly the same volume of the crystal, however, usually one set of the walls is more well-defined. Near the grain boundary this substructure contains the so-called 'S'-type bands. They are not very regular and often associated with the long dislocation walls (Fig. 6), as it was previously observed by Godfrey et al [25] also in very stable brass {110}<112>-oriented aluminium single crystals. These bands do not run through the entire crystal but their lengths, estimated from optical microscopy are of 50-500 μm (see Fig. 2a).

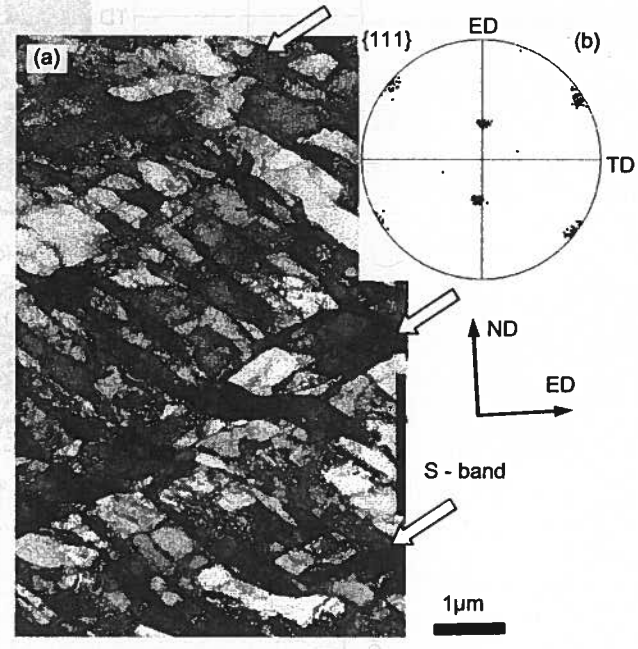

Fig. 6. 'S'-type bands in Goss-oriented crystallite. (a) TEM microstructure at the nominal deformation of 1.5, and (b) corresponding {111} pole figure. TEM local orientation measurements

3.3. SEM-FEG/EBSD orientation mapping

With the high resolution of EBSD and the high solution rate of the diffraction patterns (>95%), it is possible to study any orientation gradients that may be present along any direction of the deformation microstructure. Figure 7 shows an orientation map, made with step size of 0.1 μm, in a region near the grain boundary.

Cube-oriented crystallite. The heterogeneous strain distribution leads to strong orientation variations on a larger (millimeter) scale. On the longitudinal section the bands are usually situated along ED and separates highly and slightly dislocated areas of different orientation. In this crystals, however, a set of fine bands, inclined at 35-40° to ED, is superimposed against the background of broad deformation bands. Therefore this structure is identified as a mixture of relatively broad and thin bands oriented differently with respect to external axes. The microtexture identified within the particular areas of a cube grain shows the broad scattering of orientations mainly around TD||<100> direction. In accordance with the results obtained in TEM scale and in an earlier work [9] the crystallographic axis of <100>||TD could be regarded as a 'summary' rotation

axis of two <112>-type rotations. This finally leads the crystal lattice of the {100}<001>-initially oriented grains towards {110}<011> position, clearly visible in Fig. 7b. The inverse pole figures presented in Fig. 7c show the distribution of the external axes in crystal coordinates. The relatively large dispersion of the ND and ED axes and stabilization of the TD axis were observed.

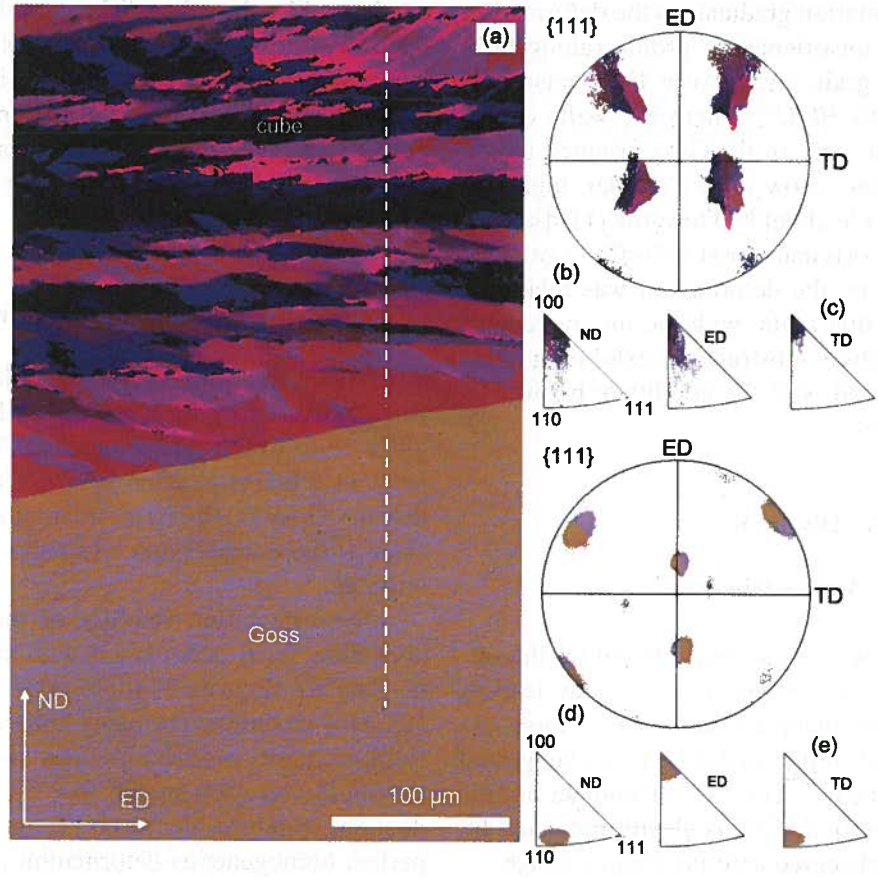

Fig. 7. (a) Orientation map from the boundary region: bottom – Goss-oriented crystallite, top – cube-oriented crystallite and corresponding distribution of orientations within: (b) and (c) cube – oriented crystallite and (d) and (e) Goss – oriented crystallite. (b) and (d) {111} pole figures, (c) and (e) inverse pole figures. SEMFEG/EBSD measurements with step size of 100 nm on longitudinal section. Sample deformed to strains of 1.5

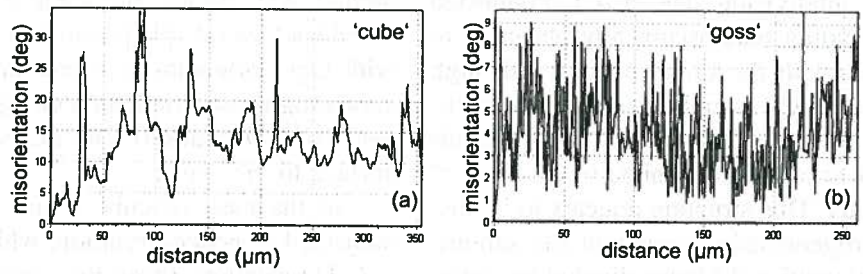

Fig. 8. Misorientation with respect to the first measured point along line scan parallel to ND. (a) Cube and (b) Goss parts of the bicrystal. SEMFEG/EBSD measurements in ND-ED plane with step size 100 nm

Goss{110}<001>-oriented crystallite. The substructure within this crystallite is significantly more homogeneous with respect to the previously discussed, excepting the thin layer near the grain boundary. The microtexture of the as-deformed Goss-oriented crystallite, presented as {111} pole figure, is shown in Fig. 7d. At deformation degree of 1.5 (68%) the high stability of this orientation is clearly observed. The orientation spread is generally less than ±10° from the initial position of {110}<001>, mainly as a result of rotation about ND.

The inverse pole figures, presented in Fig. 7e, do not show any significant dispersion tendency of the external axes either, except the above mentioned weak ND rotation. The accumulated distribution in the orientation, as indicated by dashed lines in Fig. 7a, shows the presence of localized orientation gradients in the deformation microstructures. The misorientation profile (along ND) in the cube-oriented grain shows very large misorientation angles, of up to 30-35°, where the walls of the bands are crossed (Fig. 8a). In the Goss-oriented grains the orientation gradients show a very regular, high frequency pattern and cycle about ND towards {110}<112> and back towards the original Goss{110}<001> orientation (Fig. 8b). However, the deformation was relatively homogeneous within this grain, with the microstructure developing a deformation substructure, exhibiting sinusoidal orientation spread with the amplitude below 10° and wavelength 2-5 μm.

4. Discussion

4.1. Microstructure

The results obtained in this work, based on the observation of shape and shear localizations, may lead to the conclusion that the bicrystals behave to a large extent like two individual single crystals as it was suggested previously by Z a e f f e r e r et al [15] on another bicrystalline grains configuration. This is clearly indicated by the macroscopically observed external shape change.

The difference in the characteristics of the deformation microstructure between the two crystallites may be attributed to the different combinations of slip systems in the two crystals. The detailed TEM study has clearly demonstrated the development of quite different scales of structural subdivision. The first is connected with deformation banding macroscopically observed in cube-oriented grains, with the broad bands (with high and low dislocation density) usually situated parallel (or slightly inclined) to ED, and narrow deformation bands forming microscopic substructure limited to the areas of particular broad bands. This structure appears to be distributed rather heterogeneously throughout the sample. The formation of orientational blocks divided by deformation bands can be explained in terms of the activation of alternating sets of slip systems in different regions of the crystal [26]. The third type of the structural subdivision is typically observed in Goss-oriented grains in which nearly homogeneously distributed substructure of slightly elongated subcells is formed. This substructure is only slightly disturbed in regions near the grain boundary where the formation of accommodation 'S'-type bands was observed (see Fig. 6). This is the main effect of the grain boundary influence on the deformation process observed in Goss crystallite after nominal 1.5 (68%) reduction. Also W r ó b e l et al. [27] in the intermediate layer of cold-rolled, Goss- oriented copper single crystals have find the dislocation bands which were curved and overlapped by the other dislocation bands. These curved bands were due to inhomogeneities in the strain distribution in rolling on the sample thickness. In our case these precursors of the deformation bands are induced probably by different slip systems operating within both grains near the boundary, resulting from their different initial orientation.

4.2. Microtexture

Lattice rotations within the deformed samples have been measured by high resolution EBSD mainly in regions close to the grain boundary. The texture development in a bicrystal after 1.5 (68%) reduction confirms that the Goss {110}<001> orientation is rather stable in channel-die compression while the cube {100}<001> is unstable.

The orientation stability of the Goss {110}<001> crystallite is in accordance with literature experimental data for deformed single crystal of this orientation [1]. Also modelling (by using both relaxed-constraints or full-constraints models) predicts co-planar slip of equal magnitude on each of the four systems up to 95% reduction, which results in no crystal rotation. The nearly perfect homogeneous deformation is connected with no essential change of the initial orientation and very little orientation scattering during channel-die compression. However, there are small differences in the orientation distribution between the boundary region and within the areas far from the boundary, described as a rotation around ND. Nearly the same effect was observed by W r ó b e l et al. [27] in rolled copper single crystals with Goss orientations where in the surface layers the crystallographic orientation changed systematically (as a result of ND rotation) with increasing distance from the surface to the centre.

In the case of cube grain, the crystal lattice was subjected to general rotation, which can be described as (+/-)TD rotation. From the point of view of the active slip systems, this rotation can be explained on the basis of the operation of one of two pairs of co-directional slip systems, which leads to the summary rotation about TD. The predominately TD|| <100> rotations differ from those in an earlier analysis by D i l l a m o r e and K a t o h [28], who predicted large rotations about normal (ND) and rolling (RD) directions, as well as from that of Lee et al [29] deformation banding model where the authors predicted large divergent lattice rotations about ND

and TD. However, it is well known that the observed rotations strongly depend on the applied deformation mode [30-32]. The rotation around RD being preferred to TD rotations is typically observed in rolled Al and Cu single crystals. In channel-die experiments, where widening is suppressed by the walls of the die, practically no rotations about ED were observed (rotation about TD tends to dominate). In channel-die compression Liu et al. [32] have shown that deformed cube crystals are observed to break up into macroscopic deformation bands aligned along the ED and strongly misoriented by rotation mostly about the TD with some limited ED rotations. This very well correspond to the results obtained here. It is important to note that the RD rotation in rolled samples is significantly stronger and the *'direction'* of the texture evolution strongly depends on the situation of the analysed layers on the rolled sheet thickness [27, 30]. The superposition of TD and ED(RD) rotations can leads the cube-oriented grains towards the various variants of the S-orientation, one of the well-known rolling texture components of highly rolled Al-sheets [33]. This kind of the orientation changes is predicted also by the RC Taylor type deformation model, with free $\varepsilon_{RD/ND}$ and $\varepsilon_{TD/ND}$ shears [34].

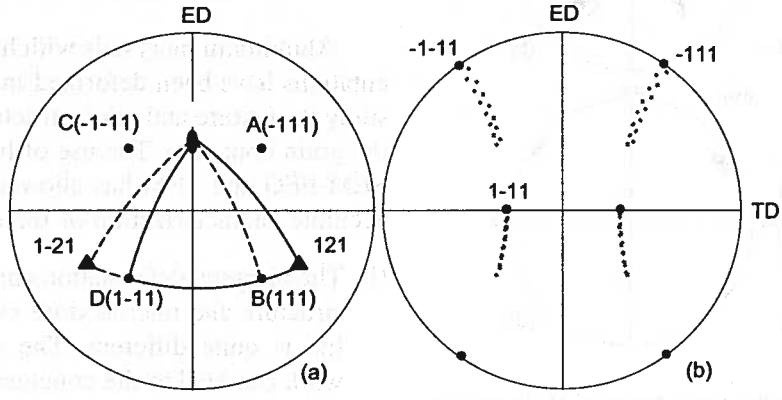

Fig. 9. (a) Stereographic projection of the cube orientation (001)[100] showing the main slip systems and the corresponding <112>-type rotation axes, (b) Schematic presentation of the rotation from (001)[100] towards (101)[10] position as a result of superposition of the two selected <112>-type rotations

A detailed description of the slip systems responsible for the analysed tendencies for scattering of the 'cube' orientation, is presented in Fig. 9. The initial orientation of the crystallite, corresponding precisely to the position of the cube(001)[100] orientation is assumed. The step-by-step crystal lattice rotation is connected with the operation of a pair of slip systems operating on A($\bar{1}11$) and C($\bar{1}\bar{1}1$) planes in the common [$\bar{1}01$] direction (co-directional pair of the slip systems) introducing the globally observed rotation about TD. Finally, these rotations lead to changes in the matrix orientation, most often observed in the performed investigations.

On macroscopic scale level, selected a combination of two from the eight possible slip systems (as is presented in Fig. 9a) can lead to the summary rotation about TD. However, only four <112> axes, lying near TD, seems to be preferable in this process. This is because (in channel-die mode of deformation) the rotation around the axes lying near ED possess limited significance. As an example, in Fig. 9b an idealized case of the sequential rotation of 4° around two axes of [$1\bar{2}1$] and [121] is shown. Finally, these partial rotations lead the cube-oriented grains towards the general final position of (101)[$\bar{1}01$]. This result is in very good agreement with the broad scattering by TD-rotations of the initial cube-orientation as obtained by X-ray diffraction or SEM/EBSD, macro- and microtexture analysis.

4.3. Effect of grain boundary

This part of the paper deals with the question, whether there is any detectable effect that might be related directly to the grain boundary. It is widely accepted that the grain boundaries act as obstacles to dislocation motion during deformation and the mechanical effect of the grain boundary depends on its misorientation. The high angle bicrystal boundary is principally non penetrable for mobile dislocations [15]. For this reason it does not promote the translation of slip from one grain to the other owing to their individual slip behaviour. This is in agreement with an earlier work by Blicharski et al [6] and Liu et al [8].

The problem of the influence of the misorientation across the grain boundary on the deformation behaviour

has been lately studied in detail by Zaefferer et al [15]. For a particular case of symmetric <112> tilt boundaries they found that for misorientations angles between grains >15°, the orientation changes were strongly attributed to dislocation pile-ups near the grain boundary.

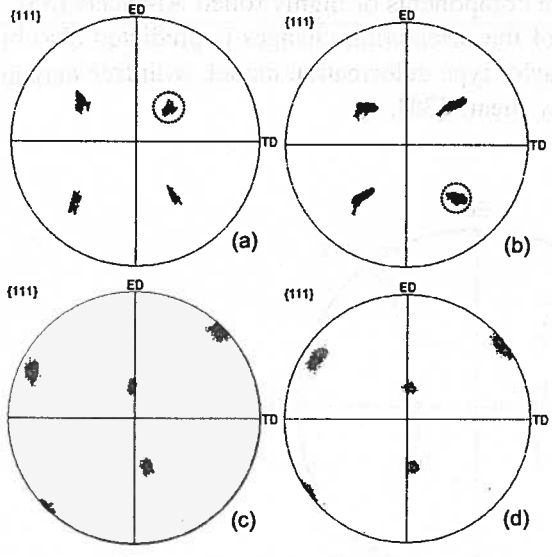

Fig. 10. {111} pole figures for the particular areas of the orientation map presented in Fig. 7a. (a) and (b) cube grain, (c) and (d) Goss-oriented grain. (a) and (c) area near grain boundary, (b) and (d) area far from boundary. SEMFEG/EBSD measurements in ND-ED plane with step size of 200 nm

Now, the orientation maps detected for areas lying near the grain boundary, are analysed again from the point of view of the different tendencies of the crystal lattice rotation near and far from the boundary, within both crystallites. At first sight, the microstructure does not show any evidence for the influence of the grain boundary on the deformation behavior. However, more significant differences in texture development are distinguished. As it has been shown, cube-oriented crystallite splits up into different orientations. The slip systems operating in the different areas of the sample influence the differences in texture scattering (Fig. 10a and b). Therefore, is very difficult to indicate significant microstructural and microtextural difference between areas lying near and far from the grain boundary. The case of the Goss-oriented crystallite shows only small variations of the crystal lattice orientation near and far from the grain boundary, mainly as a result of the reduction of the incompatibilities between grains (Fig. 10c and d). This behaviour is in opposition to the results of a previous work [9] by some of the present authors, regarding another type of the misorientation relation which occurs between the cube and the so-called hard {110}<011>-oriented grains [bicrystal with the tilt boundary of 45°<100>(||TD)]. The latter case of the grain orientation configuration shows a quite different deformation behavior, probably due to the quite different value of the Taylor factor of $\sqrt{6}$ and $2\sqrt{6}$, for cube- and hard-oriented crystallites, respectively. This implies very quick rotation of the cube grain towards {110}<011> position and the strong influence of the grain boundary on the volume of the hard-oriented crystallite lying near the boundary, where the formation of a highly deformed transition zone is observed [9].

5. Summary and conclusions

Aluminium bicrystals with high symmetry grain orientations have been deformed in channel-die in order to study the texture and microstructure development around the grain boundary. The use of high-resolution EBSD in SEM-FEG and TEM has allowed detailed and relatively accurate characterization of the deformed structures.

(i) The bicrystal deformation analysis has shown that the structure and microtexture evolution in each crystallite is quite different. The results obtained in this work can lead to the conclusion that the bicrystals in this configuration behave to a large extent like two individual single crystals.

(ii) Very strong deformation banding in the cube grain is observed and gives the initial rotation about the TD||<100>. This 'summary' rotation could be explained by superposition of two <112>-type rotations, suggesting a single {111}<110>-type slip system active in the band. The Goss {110}<011>-oriented grains are more stable under plane strain conditions and tend to develop a nearly uniform dislocation substructure.

(iii) For the strains up to 1.5 (68%) the high angle bicrystal boundary is principally non penetrable for mobile dislocations and it does not promote the translation of slip from one grain to the other owing to their individual slip behaviour. However, the initially straight boundary undergoes significant curvature and formation of the accommodation bands in Goss-oriented crystallite (near the boundary) is clearly visible.

(iv) The low amplitude and high frequency misorientations between particular small areas are detected in Goss-oriented crystallite, whereas in the cube-oriented grains only single isolated peaks of high angle boundaries across the deformation bands are observed.

(v) The present observations, together with the earlier results lead to the general conclusion that differenti-

ation in the operating slip systems in the neighbouring grains can influence their deformation behaviour near the grain boundary

REFERENCES

[1] M. Wróbel, S. Dymek, M. Blicharski, S. Gorczyca, Z. Metallkd. **85**, 415 (1994).

[2] P. Wagner, O. Engler, K. Lücke, Acta metall. mater. **43**, 3799 (1995).

[3] H. Paul, M. Darrieulat, A. Piątkowski, Z. Metallkd. **11**, 1213 (2001).

[4] H. Paul, J. H. Driver, C. Maurice, Z. Jasieński, Mat. Sci. Engn. **A359**, 178 (2003).

[5] H. W. F. Heller, C. A. Verbraak, B. H. Kolster, Acta metall. **31**, 1395 (1984).

[6] M. Blicharski, R. Becker, H. Hu, Acta metall. mater. **41**, 2007 (1993).

[7] M. C. Theyssier, J. H. Driver, Mat. Sci. Engn. **A272**, 73 (1999).

[8] Y. L. Liu, H. Hu, N. Hansen, Acta metall. mater. **43**, (1995), 2395.

[9] H. Paul, J. H. Driver, Arch. Metall. Mat. **50(1)**, 210 (2005).

[10] M. Blicharski, S. Gorczyca, Metal Sci. **12**, 3003 (1978).

[11] J. Hirsch, Mat. Sci. Techn. **6**, 1048 (1990).

[12] M. Ostafin, J. Pospiech, R. Schwarzer, Arch. Metall. Mat. **50(2)**, 409 (2005).

[13] T. J. Sabin, G. Winter, D. Juul Jensen, Acta Mat. **51**, 3999 (2003).

[14] Z. Jasieński, J. Kuśnierz, A. Piątkowski, H. Paul, J. Pospiech, A. Litwora, Arch. Metall. Mat. **44**, 422 (1999).

[15] S. Zaefferer, J-C. Kuo, Z. Zhao, M. Winning, D. Raabe, Acta Mat. **51**, 4719 (2003).

[16] F. Basson, J. H. Driver, Acta Mat. **48**, 2101 (2000).

[17] C. Rey, A. Zaui, Acta Metall. **30**, 523 (1982).

[18] J. J. Hauser, B. Chalmers, Acta metall. **9**, 802 (1961).

[19] J. D. Mote, J. E. Dorn, Trans AIME **218**, 491 (1960).

[20] T. D. Lee, H. Margolin, Metall. Trans. **8A**, 145 (1977).

[21] R. E. Hook, J. P. Hirth, Acta metall. **15**, 1099 (1967).

[22] C. Maurice, J. H. Driver, Acta metall mater. **41**, 1653 (1993).

[23] Q. Liu, J. Wert, N. Hansen, Acta mater. **48**, 4267 (2000).

[24] G. E. G. Tucker, Acta metal. **9**, 275 (1961).

[25] A. Godfrey, J. Juul Jensen, N. Hansen, Acta mater. **49**, 2429 (2001).

[26] M. Ferry, J. F. Humphreys, Mater. Sci. Forum, **Vols. 495-497**, 761 (2005).

[27] M. Wróbel, S. Dymek, M. Blicharski, S. Gorczyca, Textures and Microstructures **10**, 9 (1988).

[28] I. L. Dillamore, H. Katoh, Metal. Sci. **8**, 73 (1974).

[29] C. S. Lee, B. J. Duggan, R. E. Smallman, Acta metal. **41**, 2565 (1993).

[30] O. Engler, X. W. Kong, K. Lücke, Scripta Mater. **41**, 493 (1999).

[31] J. A. Wert, Q. Liu, N. Hansen, Acta Mater. **45**, 2565 (1997).

[32] Q. Liu, C. Maurice, J. H. Driver, N. Hansen, Metall. Trans. **29A**, 2333 (1998).

[33] O. Engler, J. Hirsch, K. Lücke, Acta metall. **37**, 2743 (1989).

[34] R. Fortunier, J. Hirsch, in Theoretical Techniques of Texture Analysis, ed. H.J. Bunge, p. 231. DGM-Verlag Oberursel (1987).

Received: 10 January 2006.